Spectroscopy With Nanostructured Superconducting Single Photon Detectors

Elisabeth Reiger, Sander Dorenbos, Valery Zwiller, Alexander Korneev, Galina Chulkova, Irina Milostnaya, Olga Minaeva, Gregory Gol'tsman, Jennifer Kitaygorsky, Dong Pan, Wojtek Słysz, Arturas Jukna, and Roman Sobolewski

Abstract—**Superconducting single-photon detectors (SSPDs) are nanostructured devices made from ultrathin superconducting films. They are typically operated at liquid helium temperature and exhibit high detection efficiency, in combination with very low dark counts, fast response time, and extremely low timing jitter, within a broad wavelength range from ultraviolet to mid-infrared (up to 6 μm). SSPDs are very attractive for applications such as fiber-based telecommunication, where single-photon sensitivity and high photon-counting rates are required. We review the current state-of-the-art in the SSPD research and development, and compare the SSPD performance to the best semiconducting avalanche photodiodes and other superconducting photon detectors. Furthermore, we demonstrate that SSPDs can also be successfully implemented in photon-energy-resolving experiments. Our approach is based on the fact that the size of the hotspot, a nonsuperconducting region generated upon photon absorption, is linearly dependent on the photon energy. We introduce a statistical method, where, by measuring the SSPD system detection efficiency at different bias currents, we are able to resolve the wavelength of the incident photons with a resolution of 50 nm.**

Index Terms—**Energy resolution, nanostructured superconducting detectors, photon spectroscopy, single-photon detectors (SPDs), superconducting SPDs (SSPDs).**

I. INTRODUCTION

INTEREST in single-photon detectors (SPDs) has recently increased dramatically, due to many novel scientific and

technical applications, ranging from studies on quantum dot single photon emitters [1] to quantum cryptography and optical quantum computing [2]. Typically, such applications require that an SPD combine several of the following properties: picosecond timing resolution (jitter), a high count rate (reaching gigahertz), almost negligible dark counts, and high quantum efficiency (QE) [3].

Silicon avalanche photodiodes (APDs) are the most popular and readily commercially available SPDs. They exhibit high QE, up to 70% at the visible (630 nm) wavelength [4]. The lowest dark count rates for commercial Si APDs are on the order of 1 Hz for ultralow noise, thermoelectrically cooled systems, and the best timing resolution can reach 40 ps, however, at the expense of a reduced QE (35% at 500 nm) [5]. Contrary to photomultiplier tubes and microchannel plates, modern Si APDs require only low biasing power, do not suffer from memory effects, and are not damaged by ambient light or overillumination. Thus, they are typically the devices-of-choice for counting visible light photons, as their QE drops dramatically at wavelengths above 1.1 μm (the value corresponding to the Si energy gap).

In the near-infrared (NIR) region, from 900 to 1700 nm, InGaAs/InP APDs operating in the Geiger mode have been widely used for photon counting. The InGaAs devices operate at near room temperature ($\sim$200 K) and possess the general robustness of solid-state devices [6]–[8]. Unfortunately, current designs suffer from strong afterpulsing and large dark count rates (on the order of 10 kHz), caused by the thermal carrier fluctuations. The best, cooled InGaAs/InP APDs operated in the short-gate mode (gate-on time $\sim$2.5 ns) exhibit QE $\sim$25% at the telecommunication 1.55 μm wavelength with a dark count probability per gate of 10^{-5} to 10^{-4}. The counting rates of InGaAs APDs are up to 20 MHz; however, their repetition rates, which assure the afterpulsing-free single-photon detection, are as low as $\sim$1 MHz, because of a long lifetime of the trapped carriers [9].

Recently, a new NIR photon-counting approach, using wavelength up-conversion in combination with a Si APD has been reported [10]. Such scheme does not require a gating operation as required for InGaAs/InP APDs, and the maximum count rate can reach 20 MHz, limited by the 45-ns value of the dead time of the Si APD.

The most promising competitors of APDs are superconducting photon detectors. They are all research devices, but they are very attractive due to low noise operation at cryogenic temperature, very high sensitivity, and the capability to count photons in the middle-infrared (MIR) range ($\sim$6 μm wavelength).

TABLE I
COMPARISON OF SEMICONDUCTING AND SUPERCONDUCTING SPDs

Detectors	Semiconducting APDs		Superconducting SPDs		
	Si [4]	InGaAs [9]	SSPD [17,19]	TES [11, 12]	STJ [13, 14]
Temperature (K)	300	200	2 - 4.2	0.1	0.4
Wavelength (μm)	0.4 - 1.1	0.9 - 1.7	0.4 - 5.6	0.1 - 5	0.2 - 1
Time resolution	300 ps	300 ps	18 ps	300 ns	< 2 ns
Quantum efficiency	70% @ 630 nm	25% @ 1.55 μm	10% @ 1.55 μm	92% @ 1.55 μm	50% @ 500 nm
Dark-count rate (Hz)	< 25	$< 10^4$	<0.01	< 0.001	N/A
Maximum count rate	10 MHz	1 MHz	250 MHz	20 kHz	50 kHz
Photon number resolution	Very limited	No	study in progress	Yes	Yes

Nano-bolometer-type, transition edge sensors (TESs) are well known and are a well-established technology. The most advanced TES devices, based on a tungsten absorber, were reported to have ~92% QE at 1.55 μm, which was obtained by embedding the TES in a specially designed resonator structure to maximize the absorption at that wavelength [11]. TESs are, unfortunately, very slow (20 kHz maximum count rate), have submicrosecond jitter, require operational temperature of ~0.1 K, and are easy to saturate by room temperature background radiation. Their advantage, besides almost perfect QE, is the ability to resolve incoming photon energy, or equivalently, the number of incident photons [12].

Superconducting tunnel junction (STJ) devices are another type of energy-resolving SPDs. They are characterized by an intrinsic spectral resolution of 20 nm, and QE is estimated to be about 50% at 500 nm [13], [14].

In 2001, yet another type of superconducting SPD (SSPD) was introduced [15], [16]. The SSPDs are nanostructured devices made from ultrathin NbN films. The active area is formed by a superconducting nanowire arranged in a meander-like geometry. They operate in the 2–4.2 K range, well below the critical temperature T_c of NbN, and are biased by a current I_b close to the nanowire critical current I_c. They exhibit single-photon sensitivity from ultraviolet to MIR [17]. Unfortunately, despite significant efforts in several laboratories worldwide, the fabrication yield of very-high-quality SSPDs is currently quite low, as those nanostructures are very sensitive to any defects and faults during the fabrication process.

Operated at 4.2 K, SSPDs typically demonstrate QE up to 20% in the visible range and ~6% in the NIR. The maximal demonstrated photon count rate of SSPDs is up to 1 GHz for small-area, low-kinetic-inductance meanders, and they show a very fast timing resolution with a time jitter <18 ps [18], [19]. Decreasing the temperature to 2 K leads to a significant improvement in QE and a drastic reduction of the dark count level. The QE of our best, large-area (100 μm²) SSPDs approached a saturation level of ~30% for visible light photons, limited by the optical absorption probability of an ultrathin NbN film. For a telecommunication wavelength of 1.3 μm, the QE at 2 K reached ~30% with a dark count rate below 2×10^{-4} Hz [17]. The maximal count rate of such large-area SSPDs is up to 250 MHz [20].

It has been shown very recently that the integration of an SSPD structure with a quarter-wavelength (λ/4) microcavity designed for the wavelength of 1.55 μm more than doubles the probability of absorbing a photon of this wavelength, and hence,

the QE reaches values as high as 57% at 1.55 μm without losing the device's high-speed characteristics [21]. Independently, single-photon sensitivity of SSPDs in the MIR was also recently observed. For the 5 μm wavelength, the detector exhibited ~1% QE at 1.6 K. We believe that actually the SSPD is capable of single-photon counting even at longer wavelengths, up to ~10 μm [22].

Table I presents a direct comparison of the performance parameters of semiconducting APDs and various superconducting SPDs.

The SSPDs are now on the verge of becoming accepted detection devices, in particular, in the NIR and MIR ranges. The first practical application of the SSPD was for noninvasive testing and debugging of CMOS integrated circuits [23], [24]. The very low timing jitter of SSPDs was recently used for fast lifetime measurements of a quantum well structure emitting in NIR [25] and in determination of the spontaneous emission lifetime of an InAs quantum dot single-photon source [26]. Low dark counts in combination with the fast recovery time, and hence, the high maximal counting rate makes SSPDs very attractive for optical communication protocols [27]. Very recently, the longest terrestrial Quantum Key Distribution (over 200 km) at 1.55 μm using a fiber link has been performed with a twin SSPD detector setup [45]. Heralding of telecommunication photon pairs [28] and photon-counting optical communications with a bit rate of 781 Mbit/s [29] were experimentally demonstrated in a combined SSPD and APD system.

There are two different ways to implement the SSPD into an optics experiment: a free space or an optical fiber-based approach. In a free-space arrangement, an optical cryostat is used in combination with a moveable lens system to focus photons directly on the SSPD chip. The setup can be used to measure QE of the detector knowing the light spot size with respect to the active area of the SSPD. Often, these QE values are given in literature (see Table I), but care has to be taken, since for real experiments, the system detection efficiency (DE) is relevant:

$$\mathrm{DE} = (P_{\mathrm{abs}} \times P_{\mathrm{det}}) \times L = \mathrm{QE} \times L \qquad (1)$$

where P_{abs} describes the probability of a photon being absorbed in the NbN film, P_{det} is the probability that an absorbed photon is leading to a detection event, and L comprises all optical losses in the setup. The product of P_{abs} and P_{det} is the QE of the device.

We have recently demonstrated pigtailing of an SSPD, where a single-mode optical fiber was glued directly on the active
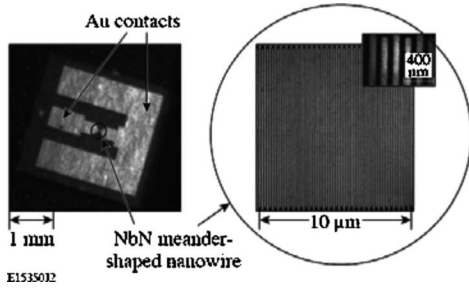
Fig. 1.   Microscope image of an SSPD detector chip (left). The active area is positioned between Au contacts. An SEM image showing the active area of the device (right). The NbN nanowire (width 100 nm, filling factor 0.5) covers the area of 10 μm $\times$ 10 μm.
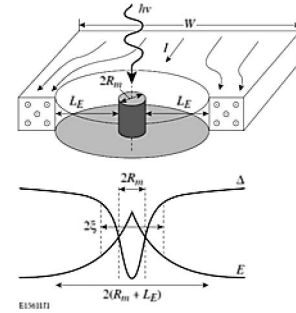

Fig. 2.   SSPD nanowire cross section with a hotspot generated by a single-photon absorption. The hotspot consists of a resistive, quasi-particle core with the diameter of the order of 2 ξ. Due to quasi-particle out-diffusion, the total final diameter of the hotspot is given by 2($\xi + L_E$). The supercurrent is expelled from the nonsuperconducting hotspot region into the strip edges, which is schematically shown by arrows.

area of the SSPD chip [20]. The main advantage of this fiber-equipped SSPD setup is that it is very easy to implement into any optics experiments. The measured DE values of the first successful fiber-coupled SSPDs are 0.3% and 1% for 1.55 and 0.9 μm photon wavelengths, respectively [20].

In this paper, we investigate the energy-resolving property of SSPDs. Due to the fact that the QE depends on the wavelength of the absorbed photon, the photon energy can be determined with the help of a statistical method. Being able not only to count individual photons, but also to gain information about their energy opens new experimental possibilities. Our "demonstration of principle" has been performed using visible light photons, but the true applicability of this concept should lie in future energy-resolving studies of single photons emitted in the infrared region.

II. DESIGN, FABRICATION, AND OPERATING PRINCIPLE

A. SSPD Design and Fabrication

SSPDs are based on 2-D superconducting nanostructures typically made from NbN films. Ultrathin (typical thickness: 2.5–10 nm) NbN films are deposited by reactive magnetron sputtering in an Ar and N$_2$ mixture on sapphire substrates. During the deposition process, the substrate is heated to 850 °C allowing epitaxial growth. The high quality of our films was demonstrated by parameters such as the surface resistance of 400–500 Ω/sq (for 4-nm-thick films), T_c of 10–11 K, and superconducting transition width of $\Delta T_c \sim 0.3$ K [30]. The active area of the SSPD is patterned by a direct electron beam lithography and reactive ion etching [31].

Fig. 1 presents a top view of an SSPD chip and an SEM image of its active area. The SSPD nanostructure is placed at a center line of a shorted, 50 Ω gold coplanar waveguide, and its active element is a superconducting nanowire with a typical width of 80–100 nm. For better coupling with the incident radiation, the nanowire is arranged in meander-type geometry. The current state-of-the-art devices are 10 μm $\times$ 0 μm meanders with a filling factor (the ratio of the area occupied by the superconducting wire to the device nominal area) as high as 0.5–0.7 [19]. For a 100-μm^2-area meander with a filling factor of 0.5, the total nanowire length is 500 μm.

B. Operating Principle: Photon Counts and Dark Counts

In the framework of a phenomenological model, the operating principle of the SSPD is based on the formation of a resistive region across a 2-D superconducting nanowire when a single photon is absorbed. This is due to a combined action of a single-photon absorption—which results in the generation of a nonsuperconducting hotspot—and redistribution of the bias current applied to the SSPD [15], [32], [33].

The absorption of a photon by a superconducting film results in breaking of a Cooper pair and generates a very hot electron, which, subsequently, looses its excess energy via electron–electron and electron–phonon interactions on a time scale of $\sim$7 ps for NbN [34]. This excess energy, if reabsorbed, leads to breaking of many additional Cooper pairs. Since the typical energy of an optical photon is about 1–2 eV, while the energy gap of 2 Δ for NbN at $T \ll T_c$ is $\sim$2 meV, the above-mentioned avalanche process leads to the creation of up to 1000 quasi-particles [35] and results in a local suppression of Δ.

The region of suppressed superconductivity is called a hotspot and has an initial diameter, or core, of 2 R_m, of the order of the superconductor coherence length ξ, as is schematically depicted in Fig. 2. This figure also shows that the diffusion of quasi-particles (diffusion length L_E) out of the resistive hotspot core causes penetration of the electric field E into the superconductor and further expands the nonsuperconducting region across the strip width. As a consequence, the supercurrent is redistributed and flows in the quasi-1-D "sidewalks." The final (total) cross-section area of the hotspot, for our 2-D superconducting strip, is approximately $\pi(R_m + L_E)^2$, and is directly related to the incident photon energy.

Indeed, numerical computations [36] based on the hotspot diffusion model developed in [33] and presented in Fig. 3 show that the hotspot cross-section area depends linearly on the photon energy in direct agreement with earlier experimental data [37]. This fact will be later used for our photon-energy-resolving measurements.

After the hotspot region has extended due to out-diffusion of quasi-particles, I_b comes into play. As schematically shown in Fig. 2, the supercurrent is redistributed around the nonsuperconducting region, leading to an increased current density j in
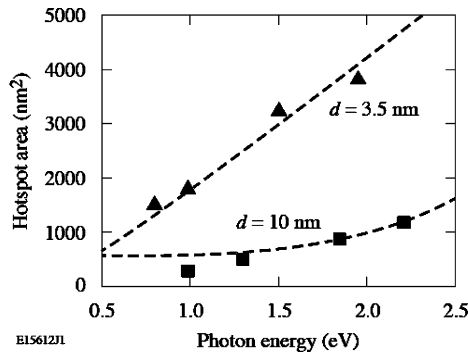
Fig. 3. Hotspot cross-section area versus the incident photon energy. The dashed lines demonstrate the hotspot dynamics and are fitted to the experimentally measured hotspot areas [37] in 3.5-nm-thick (triangles) and 10-nm-thick (squares) NbN SSPDs biased at $j/j_c = 0.9$ and operated at $T = 4.2$ K.
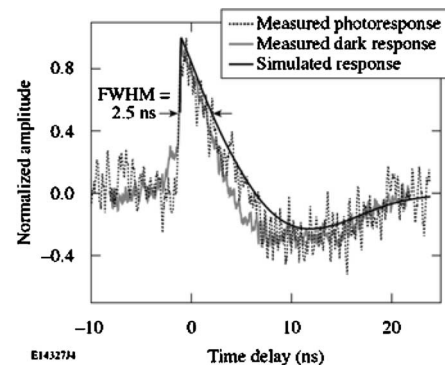

Fig. 4. Measured photoresponse signal (dotted line) of a 100 μm^2 area fiber-coupled SSPD compared with a theoretical calculation (dark solid line), based on the kinetic inductance model [40]. The shown dark count photoresponse (light solid line) is almost identical to the photon absorption signal.

the 1-D sidewalks near the edge of the strip. Once the critical current density j_c in those "sidewalks" is exceeded, phase-slip centers (PSCs) form, and as a consequence, a resistive region across the entire width of the detector nanostrip is formed. This latter process is time-delayed with respect to the initial hotspot generation and was investigated in detail in [38].

The processes of the hotspot and PSCs formation can quantitatively explain both the SSPD time jitter and the QE dependence on the photon energy. It is clear that the hotspot size and the nanowire width uniformity are critical in determining the intrinsic jitter and QE of the device. Any variations of the strip width directly affect j_c of the entire device with the narrowest segment of the meander setting the upper limit on the maximal I_b. Hence, only some (narrowest) parts of the nanowire are optimally current biased, while for wider parts (with $I_b \ll I_c$), the formation of a resistive region becomes significantly less probable. As expected, devices with improved strip uniformity exhibit high QEs and the lowest experimentally observed time jitter values <20 ps [18].

Superconductivity of the resistive region is restored due to the recombination of excited quasi-particles in combination with out-diffusion of phonons [39]. For an ultrathin NbN superconducting film, the quasi-particle relaxation time is ~30 ps [34]; thus, on this time scale, the hotspot is expected to collapse and superconductivity be restored. This intrinsic recovery time, together with the time delay for forming the resistive (PSC) barrier, sets the maximal, intrinsic counting rate of up to ~10 GHz [18]. However, it has been recently shown by Kerman *et al.* [40] that the SSPD response time is limited by another parameter, namely, the kinetic inductance of a superconducting meander. The kinetic inductance effect is intrinsic to any nanostructured superconducting devices; it typically exceeds the value of the geometrical inductance, and depends on the thickness and the width of the superconducting nanowire. The thinner, narrower, and longer the nanowire is, the higher is its superconducting kinetic inductance. Hence, there is a tradeoff between the maximal count rate and the maximal QE value for large-active area (large-meander) devices. As a consequence, the recent SSPDs with active areas of 100 μm^2 exhibit the largest QE values, but their maximal count rates are below 250 MHz [20].

Fig. 4 shows a photoresponse signal (dotted line) of a 100-μm^2 -area, 0.6-filling-factor SSPD, recorded using a 6 GHz Tektronix, single-shot digital oscilloscope. The experimentally measured transient has a full-width at half-maximum of about 2.5 ns and exhibits a small negative tail component due to the limited (50 MHz to 4 GHz) bandwidth of the amplifier. Obviously, the presented transient in Fig. 4 does not represent the intrinsic photoresponse of the superconducting material (NbN) that, as we mentioned before, is of the order of 30 ps, but is limited by the kinetic inductance of the ~0.5-mm-long nanowire meander. The observed pulse shape is in good agreement with our numerical simulations (solid line) based on the kinetic inductance, taking into account the acquisition electronics bandwidth [41].

Even when the SSPD is completely blocked from all incoming radiation, one can still observe sporadic voltage pulses. It has been suggested that these dark counts are due to the depairing of vortex–antivortex pairs caused by the applied bias current [42], [43]. The photoresponse of dark counts is very similar to the signal caused by single photon absorption (see Fig. 4, light solid line) with the pulsewidth also set by the kinetic inductive effect. The dark count rates decrease exponentially with decreasing I_b and can be significantly reduced by going to low (well below 4.2 K) operating temperatures [17].

Finally, we would like to note that the fact that in large-area SSPDs, the photoresponse is limited by the kinetic inductive effect contradicts proposals for single-shot photon-energy-resolving measurements [33], [44], based on the assumption that both the height and duration of the SSPD photoresponse pulse should be dependent on the energy of the absorbed photon.

III. EXPERIMENTAL SETUP

In Fig. 5, we present our fiber-based setup used for demonstrating the energy-resolving properties of SSPDs. We use a simple dip-stick design to immerse the detector in liquid He. The detector is positioned well below the liquid He surface, ensuring a stable operating temperature of 4.2 K.

The SSPD had an active area of 10 μm $\times$ 10 μm with a filling factor of 0.5 and a nominal strip width of 100 nm. The SSPD
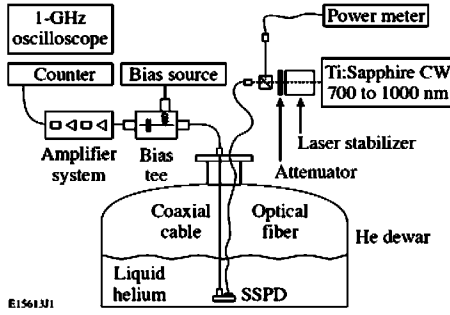
Fig. 5. Sketch of a fiber-coupled SSPD setup. The detector was immerged in liquid He inside a transport He dewar using a simple dipstick design. The bias current was applied via a dc port of a bias tee. The SSPD transient was amplified and detected by a pulse counter. The laser light was delivered to our SSPD through an optical fiber.
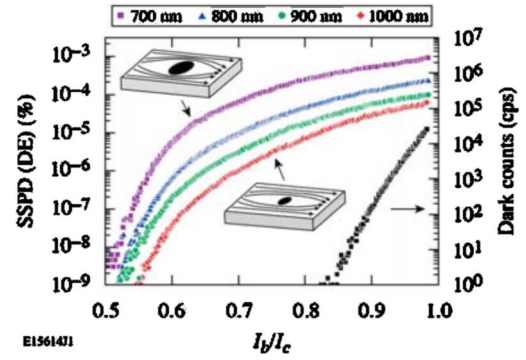

Fig. 6. Bias current scans for different incident photon wavelengths. The SSPD system DE strongly depends on the energy of the absorbed photons. It is highest for 700 nm photons due to the large diameter of the generated nonsuperconducting hotspot and lowest for the longest wavelength of 1000 nm, as illustrated schematically by the two insets. The right-hand axis corresponds to the dark count rate of the SSPD, represented by black dots.

was pigtailed with a P1-SMF28 fiber (Thorlabs, single mode: 1310–1550 nm) following the procedure presented in [20].

The electronic readout system was placed outside the He dewar at room temperature. The bias current was generated by a computer-controlled data acquisition unit (National Instruments, DAQPad-6015) in combination with a 440 kΩ resistor and applied via the dc-port of a home-made bias tee (bandwidth: 1 MHz–5 GHz). The RF port of the bias tee was connected to an amplifier cascade of two low-noise amplifiers (Miteq, JS2-01000200-10-10A, gain 36 dB). Two attenuators (10 dB), one placed between the amplifiers and the other after the second amplifier, were used for stabilizing the amplifier cascade and to minimize back actions from the pulse counter. The SSPD response (amplified voltage pulses) was fed to a counter (Stanford Research, SR400 Photon Counter) or monitored with a 1 GHz oscilloscope (LeCroy, LC574AM).

Assuming that the resistance of the SSPD when it was in its resistive state, R_{SSPD}, was much higher than the 50 Ω input impedance of the amplifier, the measured amplitude of the voltage photoresponse pulse was expected to be $V_{\mathrm{pulse}} \approx I_b \times 50\Omega \times G_{\mathrm{sig}}$, where G_{sig} is the total gain of the amplifier system within the amplifier passband [40]. The measured I_c of our SSPD was $\sim$11.8 μA, and a typical photoresponse pulse had a amplified voltage amplitude of $\sim$250 mV, when the SSPD was biased with $I_b/I_c = 0.8$.

For demonstrating energy-resolving properties of the SSPD, we used a tunable Ti:sapphire laser (Coherent, MIRA900) with a wavelength range between 700 and 1000 nm as a photon source. The laser was operated in a continuous-wave mode. To monitor the laser stability and to be able to compensate for possible light intensity fluctuations, a beam splitter was positioned between the laser output and the fiber coupler, and the intensity was constantly monitored by a power meter (Thorlabs, S120A), together with the SSPD readout. No collimation optics was used to focus the incident light onto the fiber input. The aforementioned coupling arrangement minimized the setup sensitivity with respect to the laser spot variations and was expected to assure minimal changes in the coupling efficiency for different wavelengths used in the experiment. On the other hand, it forced us to apply high incident laser powers to obtain high-count photon rates from the SSPD. The laser intensity was varied using a laser

stabilization system (Brockton Electrooptic Corporation) and a calibrated attenuator wheel in front of the beam splitter.

IV. PHOTON-ENERGY-RESOLVING PROPERTY

To gain information about the energy of absorbed single photons, we use the fact that, for a given thickness of a NbN nanowire, the area of a nonsuperconducting hotspot depends linearly on the energy of the incident photon (cf., Fig. 3). In the case of a 10-nm-thick SSPD, the difference in the hotspot diameters is 30%, when comparing the hotspot sizes corresponding to the 700-nm (hotspot diameter $\sim$25 nm) and 1000-nm ($\sim$32 nm) wavelength photons. For 4-nm-thick devices used in our experiments, we follow the dependence presented in Fig. 3 for a 3.5-nm-thick SSPD, assuming actual differences between the nominally 3.5 and 4 nm nanowires are negligible.

Fig. 6 presents a family of the system DE curves versus the normalized applied bias current, collected for different incident photon wavelengths. Clearly, it can be seen that, for shorter wavelengths, larger DEs are obtained for the same I_b, because highly energetic photons create larger hotspots, and the condition for the PSC generation in the sidewalks can be fulfilled for lower I_b values. For example, at $I_b/I_c = 0.7$, the difference in the DEs values for the 700 and 1000 nm photons is approximately two orders of magnitude. For the 700 nm wavelength, the DE is almost saturated, whereas for 1000 nm photons, DE could still be further increased by going closer toward I_c.

For the studied SSPD, the overall system DE presented in Fig. 6 is rather low. One apparent reason is that the optical coupling of the laser light to the SSPD used in our experiments is far below the best, $\sim$30% value, reported for the best pigtailed SSPD and more comparable with the other, tested devices [20]. In addition, the device QE in this particular SSPD might be reduced, possibly due to, e.g., variations of the nanowire strip width. Nevertheless, despite the very low absolute DE values, the DE curves collected for different wavelengths are very reproducible and generally typical for SSPDs, showing a strong dependence on the energy of the incident photons. The latter is
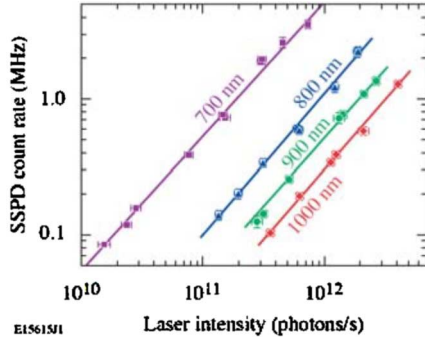
Fig. 7. Photon-count rate dependence on the laser intensity. The linear dependence is the prerequisite to be able to recalibrate test curves taken at arbitrary intensities and compare them to the calibration curves.

Fig. 8. Calibration curves. For wavelengths from 700 to 1000 nm in steps of 50 nm, I_b was scanned from 6.8 to 11.4 μA at 45 nA steps. All curves are normalized to 10^6 Hz at $I_b = 10.2$ μA to simplify the fitting procedure. The original data (solid squares) and the normalized data (circles) of one test curve taken at arbitrary laser intensity are shown. The recalibrated test data can be clearly assigned to the 1000 nm calibration curve.

crucial for our demonstration of single-photon energy resolution ability of SSPDs.

The right-hand axis in Fig. 6 corresponds to the dark count rate of the SSPD, measured (black dots) when the laser light was completely blocked. We note that the dark counts are relevant only for $I_b/I_c > 0.85$. But even then, they are relatively low, despite the fact that we did not properly shield our device from the thermal background radiation (there were no cold IR filters in our optical beam line).

For our proposed fitting procedure, the second criterion that has to be fulfilled is the linear dependence of the SSPD photon-count rate on the incident photon flux (laser intensity), as we presume that we cannot fully control the intensity of the light source for which we want to determine the photon wavelength. Thus, the actual measured photon-count rate has to be normalized with respect to the calibration curves, which were obtained at a known wavelength and at a given intensity. In Fig. 7, the linear dependence of the SSPD count rate is shown with the laser intensity varied over two orders of magnitude. This linear dependence is expected, unless the laser power is increased to very high values, where we leave the one-photon absorption regime [37]. In fact, the linear dependence of photon counts on the number of incoming photons for very weak photon fluxes is a direct confirmation of the single-photon-counting nature of our detectors [15].

A. Fitting Procedure

Calibration curves were taken for different laser wavelengths over the whole tunable wavelength regime from 700 to 1000 nm in steps of 50 nm, as presented in Fig. 8. The laser intensity of each calibration curve was chosen in such a way that at the 10.2 μA bias level, the obtained photon-count rate was approximately 1 MHz. The I_b step size was 45 nA. For each point, the count rate was measured for 1 s. Several calibration curves for each wavelength were taken, normalized to exactly 10^6 Hz at $I_b = 10.2$ μA and averaged, resulting in a relative error of no more than 1% (error bars not shown in Fig. 8).

For demonstrating the energy-resolving property, we have taken our test curves at the same wavelengths as the calibration curve, but measured for arbitrary intensities of incident photons. The photon-count rate of the SSPD was measured at four dif-
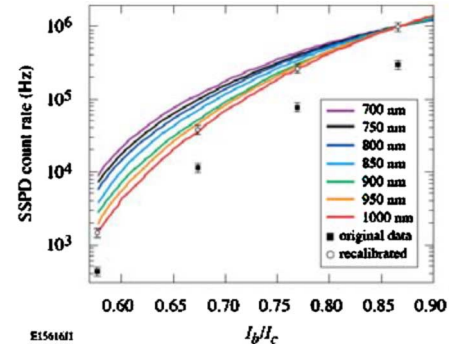
ferent I_b settings (6.8, 8.0, 9.1, and 10.2 μA). Each data point was an average over 20 measurements, each one taken for 1 s. The total time needed for taking one test curve was about 1–2 min. The value at 10.2 μA was used to normalize the given test curve with respect to the calibration curve to the 10^6 Hz count value. In Fig. 8, both the original and the normalized points of one of the test curve are plotted. It can be easily assigned by eye to the calibration curve of 1000 nm wavelength.

B. Fitting Results

For a quantitative assignment, we calculated the sum of the squared differences of all points of one test curve (x_i) with respect to all calibration curves $[\mathrm{cal}_i(j)]$, with (j) being different wavelengths:

$$\mathrm{sum}(j) = \sum \frac{(x_i - \mathrm{cal}_i(j))^2}{\mathrm{cal}_i(j)}. \tag{2}$$

By finding the minimum value of $\mathrm{sum}(j)$, the actual wavelength of the test curve could be determined [cf., Fig. 9(b)]. We have tested our fitting procedure on 14 test curves. For each wavelength (i.e., 700, 750, . . . , 1000 nm), two test curves were measured at different laser intensities [only odd test data are listed in Fig. 9(b)]. All except one test curve could be assigned to the correct wavelength. Contrary to Fig. 9(b), which presents the raw test data, in Fig. 9(a), we plotted the values of $\mathrm{sum}(j)$ for each of 14 tests, normalized with respect to their corresponding minimum values [bold numbers listed in Fig. 9(b) for odd test curves]. For all expect one curve, a relative difference higher than 5 [Fig. 9(a), dotted line] was obtained, and the wavelength could be assigned with very high certainty. Problems arise only in the case of one, 1000 nm test curve, where, for two calibration curves, the relative squared difference was too small to make a clear wavelength assignment.

The measurement must be free of any external disturbances, such as bias current fluctuations or drift and/or laser fluctuations on the time scale much smaller than 1 s, which could not be completely compensated in our experiments. In particular, at $I_b = 10.2$ μA, which was used for recalibration, the measure-
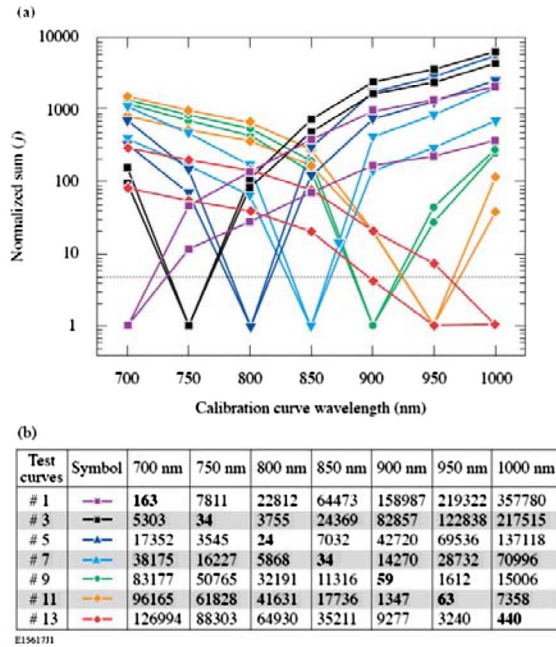
(a)

(b)

Test curves	Symbol	700 nm	750 nm	800 nm	850 nm	900 nm	950 nm	1000 nm
# 1	–■–	**163**	7811	22812	64473	158987	219322	357780
# 3	–■–	5303	**34**	3755	24369	82857	122838	217515
# 5	–▲–	17352	3545	**24**	7032	42720	69536	137118
# 7	–▲–	38175	16227	5868	**34**	14270	28732	70996
# 9	–●–	83177	50765	32191	11316	**59**	1612	15006
# 11	–●–	96165	61828	41631	17736	1347	**63**	7358
# 13	–●–	126994	88303	64930	35211	9277	3240	**440**

Fig. 9.   Wavelength assignment for all 14 test curves. For each test curve, sum(j) with respect to all calibration curves is calculated (cf., table). The normalized squared difference for each test curve is plotted versus the calibration curves. For all curves, except one, there is a clear minimum value of sum(j) and the photon wavelength can be assigned with high certainty. The dotted line represents a relative difference of 5, which is used as threshold for an unambiguous assignment.

ments are very sensitive to any disturbance. Therefore, for an unambiguous photon energy assignment, a threshold value of the factor of 5 for the difference between the relative squared differences was used. We stress that this latter condition is satisfied for all test curves except for one of the two 1000 nm curves. In general, the procedure should be that, if the aforementioned threshold is not reached, then simply the measurement of the given test curve has to be repeated until the criterion is fulfilled.

In our procedure, the energy information about the incident photons is obtained statistically, i.e., we have to measure the photon-count rate for at least two different bias current settings. That requires a stable light source over the time needed for performing the bias scan, which is 1–2 min in our case, when using four different I_b values. By reducing the number of points and the amount of averaging, this acquisition time can be lowered, however, at the cost of accuracy.

We have also tested an approach, where test curves were taken with a smaller I_b step size. We determined the slope of the test curve and compared it with the slope of the calibration curves. However, the results of this method were not as accurate as for the four-point measurements discussed previously, presumably because we had to reduce the averaging time for each measurement point in order to achieve a total measurement time in the same 1–2 min range.

Detector instabilities, which could cause slightly different count rates under exactly the same experimental conditions were, probably, the main reason for the observed 50 nm wavelength resolution limit of our method. When taking calibration
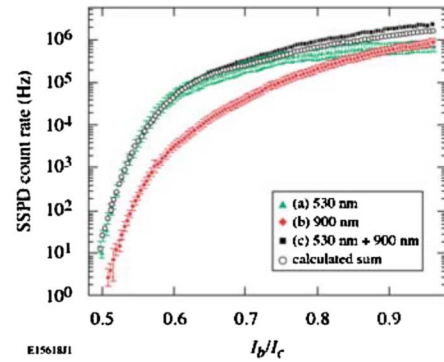

Fig. 10.   Wavelength assignment for a light source composed of two different wavelengths. The count rate of only the green laser (a), only the IR laser (b), and of both lasers simultaneously (c) are shown together with the calculated sum of (a) and (b) (open circles).

curves with smaller wavelength step size, the error bars of the calibration curves started to overlap. By using an SSPD with somewhat higher DE, and a better shielded readout system, our energy resolution should be substantially improved.

C. Light Source With Two Different Wavelengths

Our photon-energy-resolving approach should also work in the case of an incident optical flux consisting photons with two different energies. Using our method, we should be able to determine the wavelengths, as well as the intensities of both contributions. To show the proof of principle, we equipped our setup with a single-mode fiber optic coupler (Thorlabs, 10202A-50-FC) and used the pump laser of our system (Coherent, Verdi: 530 nm) as the source of one (green) wavelength radiation, while the Ti:sapphire laser at a wavelength of 900 nm was the second source of photons.

Fig. 10 presents the photon-count rates obtained for three different cases: 1) only the green (530 nm) laser was connected to the input fiber of the SSPD, 2) only the IR wavelength beam of the Ti:sapphire laser was used, and finally, 3) both beams were coupled in at the same time and fed to the SSPD. Additionally, Fig. 10 shows the calculated sum (open circles) of the curves in Fig. 10(a) and (b).

At low values of I_b, the count rate curve [Fig. 10(c)], when photons of both wavelengths are incident on the SSPD, is dominated by the contribution of the green laser. This is due to the fact that the SSPD DE is much higher for green photons as compared to that of IR photons. As a consequence, the low I_b/I_c regime, e.g., 0.5–0.6, can be used for determining the wavelength of the high-energy photons, as well as to measure their flux. Taking this information into account, a fit of the count rate curve with the calibration curves in a bias current window close to the critical current (0.8–0.9) gives the wavelength and intensity of the low-energy photons. Note that for I_b close to I_c, the count rate of the green laser [Fig. 10(a)], as well as the count rate of the Ti:sapphire laser [Fig. 10(b)], differ significantly from curve Fig. 10(c). Only the sum of both with the correct ratio of the intensities will give the observed count rate curve in Fig. 10(c).

Fig. 10 demonstrates that the careful analysis of the measured photon-count curves in separated I_b/I_c windows, and their direct comparison with the prerecorded calibration curves can allow to obtain accurate energy determination also in case the incident light consists of photons of different energies.

V. CONCLUSION

SSPDs are a very promising type of solid-state SPDs, due to their efficient photon counting, especially in the NIR-to-MIR region, almost negligible dark counts, the low timing jitter, and finally, megahertz-to-gigahertz photon-counting rates. The properties mentioned before make SSPDs very attractive in such basic science applications as single-photon emission studies and time-resolved correlation measurements in the infrared, as well as in the engineering requiring very high counting rates and ranging from fiber-based and free-space quantum communications to quantum cryptography. We have demonstrated that, besides their photon-counting abilities, SSPDs can also be used in the photon-energy-resolution mode. We used the fact that the detection efficiency (DE) depends on the energy of the absorbed photons and demonstrated an energy resolution of 50 nm for a monochromatic light source. We expect that our energy resolution concept can become practical by implementing detectors with higher system DE values and applying it to spectral studies of IR photon sources. In fact, we can envision a very compact single-photon spectroscopy setup, e.g., an on-chip design, where the SSPD and a quantum dot embedded in a nanowire acting as a single-photon source are integrated on the same substrate.

ACKNOWLEDGMENT

REFERENCES

[1] V. Zwiller, H. Blom, P. Jonsson, N. Panev, S. Jeppesen, T. Tsegaye, E. Goobar, M.-E. Pistol, L. Samuelson, and G. Björk, "Single quantum dots emit single photons at a time: Antibunching experiments," *Appl. Phys. Lett.*, vol. 78, pp. 2476–2478, 2001.

[2] J. C. Livas, E. A. Swanson, S. R. Chinn, and S. Kintzer, in *Free-Space Laser Communication Technologies VII*, vol. 2381, G. S. Mecherle, Ed. Bellingham, WA: SPIE, 1995, p. 38.

[3] C. Kurtsiefer, P. Zarda, Ph.M. Halder, M. Gorman, P. R. Tapster, J. G. Rarity, and H. Weinfurter, "Long-distance free-space quantum cryptography," in *Quantum Optics in Computing and Communications*, vol. 4917, S. Liu, G. Guo, H.-K. Lo, and N. Imoto, Eds. Bellingham, WA: SPIE, 2002, pp. 25–31.

[4] SPCM-AQR-16-FC—Si APD single photon counting module with <25 dark counts/second (2007). [Online]. Available: http://optoelectronics. perkinelmer.com

[5] id100 (2007). [Online]. Available: http://www.idquantique.com

[6] A. Tomita and K. Nakamura, "Balanced, gated-mode photon detector for quantum-bit discrimination at 1550 nm," *Opt. Lett.*, vol. 27, no. 20, pp. 1827–1829, 2002.

[7] G. Ribordy, N. Gisin, O. Guinnard, D. Stucki, M. Wegmuller, and H. Zbinden, "Photon counting at telecom wavelengths with commercial In-GaAs/InP avalanche photodiodes: Current performance," *J. Mod. Opt.*, vol. 51, pp. 1381–1398, 2004.

[8] A. Yoshizawa, R. Kaji, and H. Tsuchida, "Gated-mode single-photon detection at 1550 nm by discharge pulse counting," *Appl. Phys. Lett.*, vol. 84, pp. 3606–3608, 2004.

[9] id201 (2007). [Online]. Available: http://www.idquantique.com

[10] C. Langrock, E. Diamanti, R. V. Roussev, Y. Yamamoto, and M. M. Fejer, "Highly efficient single-photon detection at communication wavelengths by use of upconversion in reverse-proton-exchanged periodically poled LiNbO$_3$ waveguides," *Opt. Lett.*, vol. 30, pp. 1725–1727, 2005.

[11] D. Rosenberg, A. E. Lita, A. J. Miller, and S. W. Nam, "Noise-free high-efficiency photon-number-resolving detectors," *Phys. Rev. A*, vol. 71, pp. 061803-1–061803-4, 2005.

[12] A. J. Miller, S. W. Nam, J. M Martinis, and A. V. Sergienko, "Demonstration of a low-noise near-infrared photon counter with multiphoton discrimination," *Appl. Phys. Lett.*, vol. 83, pp. 791–793, 2003.

[13] A. Peacock, P. Verhoeve, N. Rando, A. van Dordrecht, B. G. Taylor, C. Erd, M. A. C. Perryman, R. Venn, J. Howlett, D. J. Goldie, J. Lumley, and M. Wallis, "Single optical photon detection with a superconducting tunnel junction," *Nature*, vol. 381, pp. 135–137, 1996.

[14] D. D. E. Martin, P. Verhoeve, A. Peacock, A. van Dordrecht, J. Verveer, and R. Hijmering, "A 12 × 10 pixels superconducting tunnel junction array based spectro-photometer for optical astronomy," *Nucl. Instrum. Methods Phys. Res.*, vol. 520, pp. 512–515, 2004.

[15] G. Gol'tsman, O. Okunev, G. Chulkova, A. Lipatov, A. Semenov, K. Smirnov, B. Voronov, A. Dzardanov, C. Williams, and R. Sobolewski, "Picosecond superconducting single-photon optical detector," *Appl. Phys. Lett.*, vol. 79, pp. 705–707, 2001.

[16] R. Sobolewski, A. Verevkin, G. N. Gol'tsman, A. Lipatov, and K. Wilsher, "Ultrafast superconducting single-photon optical detectors and their applications," *IEEE Trans. Appl. Supercond.*, vol. 13, no. 2, pp. 1151–1157, Jun. 2003.

[17] A. Korneev, V. Matvienko, O. Minaeva, I. Milostnaya, I. Rubtsova, G. Chulkova, K. Smirnov, B. Voronov, G. Gol'tsman, W. Słysz, A. Pearlman, A. Verevkin, and R. Sobolewski, "Quantum efficiency and noise equivalent power of nanostructured, NbN, single-photon detectors in the wavelength range from visible to infrared," *IEEE Trans. Appl. Supercond.*, vol. 15, no. 2, pp. 571–574, Jun. 2005.

[18] A. Pearlman, A. Cross, W. Słysz, J. Zhang, A. Verevkin, M. Currie, A. Korneev, P. Kouminov, K. Smirnov, B. Voronov, G. Gol'tsman, and R. Sobolewski, "Gigahertz counting rate of NbN single-photon detectors for quantum communication," *IEEE Trans. Appl. Supercond.*, vol. 15, no. 2, pp. 579–582, Jun. 2005.

[19] A. Korneev, P. Kouminov, V. Matvienko, G. Chulkova, K. Smirnov, B. Voronov, G. N. Gol'tsman, M. Currie, W. Lo, K. Wilsher, J. Zhang, W. Słysz, A. Pearlman, A. Verevkin, and R. Sobolewski, "Sensitivity and gigahertz counting performance of NbN superconducting single-photon detectors," *Appl. Phys. Lett.*, vol. 84, no. 26, pp. 5338–5340, 2004.

[20] W. Słysz, M. Wegrzecki, J. Bar, M. Górska, V. Zwiller, C. Latta, P. Bohi, I. Milostnaya, O. Minaeva, A. Antipov, O. Okunev, A. Korneev, K. Smirnov, B. Voronov, N. Kaurova, G. Gol'tsman, A. Pearlman, A. Cross, I. Komissarov, A. Verevkin, and R. Sobolewski, "Fiber-coupled single-photon detectors based on NbN superconducting nanostructures for practical quantum cryptography and photon-correlation studies," *Appl. Phys. Lett.*, vol. 88, pp. 261113-1–261113-3, Jun. 2006.

[21] K. M. Rosfjord, J. K. W. Yang, E. A. Dauler, A. J. Kerman, V. Anant, B. M. Voronov, G. N. Gol'tsman, and K. K. Berggren, "Nanowire single-photon detector with an integrated optical cavity and anti-reflection coating," *Opt. Exp.*, vol. 14, pp. 527–534, Jan. 2006.

[22] G. Gol'tsman, O. Minaeva, A. Korneev, M. Tarkhov, I. Rubtsova, A. Divochiy, I. Milostnaya, G. Chulkova, N. Kaurova, B. Voronov, D. Pan, J. Kitaygorsky, A. Cross, A. Pearlman, I. Komissarov, W. Słysz, M. Wegrzecki, P. Grabiec, and R. Sobolewski, "Middle-infrared to visible-light ultrafast superconducting single-photon detector," *IEEE Trans. Appl. Supercond.*, vol. 17, no. 2, pp. 246–251, 2007.

[23] J. Zhang, N. Boiadjieva, G. Chulkova, H. Deslandes, G. N. Gol'tsman, A. Korneev, P. Kouminov, M. Leibowitz, W. Lo, R. Malinsky, O. Okunev, A. Pearlman, W. Słysz, A. Verevkin, K. Wilsher, C. Tsao, and R. Sobolewski, "Non-invasive CMOS circuit testing with NbN superconducting single-photon detectors," *Electron. Lett.*, vol. 39, no. 14, pp. 1086–1088, Jul. 2003.

[24] S. Somani, S. Kasapi, K. Wilsher, W. Lo, R. Sobolewski, and G. N. Gol'tsman, "New photon detector for device analysis: Superconducting single-photon detector based on a hot electron effect," *J. Vac. Sci. Technol. B*, vol. 19, no. 6, pp. 2766–2769, 2001.

[25] M. J. Stevens, R. H. Hadfield, R. E. Schwall, S. W. Nam, R. P. Mirin, and J. A. Gupta, "Fast lifetime measurements of infrared emitters using a low-jitter superconducting single-photon detector," *Appl. Phys. Lett.*, vol. 89, pp. 031109-1–031109-3, Jul. 2006.

[26] R. H. Hadfield, M. J. Stevens, S. S. Gruber, A. J. Miller, R. E. Schwall, R. P. Mirin, and S. W. Nam, "Single photon source characterization with a superconducting single photon detector," *Opt. Exp.*, vol. 13, no. 26, pp. 10846–10853, 2005.

[27] R. H. Hadfield, J. L. Habif, J. Schlafer, R. E. Schwall, and S. W. Nam, "Quantum key distribution at 1550 nm with twin superconducting single-photon detectors," *Appl. Phys. Lett.*, vol. 89, pp. 241129-1–241129-3, Dec. 2006.

[28] M. A. Jaspan, J. L. Habif, R. H. Hadfield, and S. W. Nam, "Heralding of telecommunication photon pairs with a superconducting single photon detector," *Appl. Phys. Lett.*, vol. 89, pp. 031112-1–031112-3, 2006.

[29] B. S. Robinson, A. J. Kerman, E. A. Dauler, R. J. Barron, D. O. Caplan, M. L. Stevens, J. J. Carney, S. A. Hamilton, J. K. W. Yang, and K. K. Berggren, "781 Mbit/s photon-counting optical communications using a superconducting nanowire detector," *Opt. Lett.*, vol. 31, no. 4, pp. 444–446, Feb. 2006.

[30] S. Cherednichenko, P. Yagoubov, K. Il'in, G. Gol'tsman, and E. Gershenzon, "Large bandwidth of NbN phonon cooled hot electron bolometer mixers on sapphire substrates," in *Proc. 8th Int. Symp. Space Terahertz Technol.*, Boston, MA, 1997, p. 245.

[31] G. N. Gol'tsman, K. Smirnov, P. Kouminov, B. Voronov, N. Kaurova, V. Drakinsky, J. Zhang, A. Verevkin, and R. Sobolewski, "Fabrication of nanostructured superconducting single-photon detectors," *IEEE Trans. Appl. Supercond*, vol. 13, no. 2, pp. 192–195, Jun. 2003.

[32] A. Verevkin, A. Pearlman, W. Słysz, J. Zhang, M. Currie, A. Korneev, G. Chulkova, O. Okunev, P. Kouminov, K. Smirnov, B. Voronov, G. N. Golt'sman, and R. Sobolewski, "Ultrafast superconducting single-photon detectors for near-infrared-wavelength quantum communications," *J. Mod. Opt*., vol. 51, no. 9/10, pp. 1447–1458, 2004.

[33] A. D. Semenov, G. N. Gol'tsman, and A. A. Korneev, "Quantum detection by current carrying superconducting film," *Physica C*, vol. 351, pp. 349–356, 2001.

[34] K. S. Il'in, M. Lindgren, M. Currie, A. D. Semenov, G. N. Gol'tsman, R. Sobolewski, S. I. Cherednichenko, and E. M. Gershenzon, "Picosecond hot-electron energy relaxation in NbN superconducting photodetectors," *Appl. Phys. Lett.*, vol. 76, pp. 2752–2754, 2000.

[35] K. S. Il'in, I. I. Milostnaya, A. A. Verevkin, G. N. Gol'tsman, E. M. Gershenzon, and R. Sobolewski, "Ultimate quantum efficiency of a superconducting hot-electron photodetector," *Appl. Phys. Lett.*, vol. 73, pp. 3938–3940, 1998.

[36] A. Jukna (2006). private communication.

[37] A. Verevkin, J. Zhang, R. Sobolewski, A. Lipatov, O. Okunev, G. Chulkova, A. Korneev, K. Smirnov, G. N. Gol'tsman, and A. Semenov, "Detection efficiency of large-active-area NbN single-photon superconducting detectors in the ultraviolet to near-infrared range," *Appl. Phys. Lett.*, vol. 80, no. 25, pp. 4687–4689, Jun. 2002.

[38] J. Zhang, W. Słysz, A. Pearlman, A. Verevkin, R. Sobolewski, O. Okunev, G. Chulkova, and G. Gol'tsman, "Time delay of resistive-state formation in superconducting stripes excited by single optical photons," *Phys. Rev. B*, vol. 67, pp. 132508-1–132508-4, 2003.

[39] A. Semenov, G. N. Gol'tsman, and R. Sobolewski, "Hot-electron effect in superconductors and its applications for radiation sensors," (topical review article), *Supercond. Sci. Technol.*, vol. 15, pp. R1–R16, 2002.

[40] A. J. Kerman, E. A. Dauler, W. Keicher, J. K. W. Yang, K. K. Berggren, G. Gol'tsman, and B. Voronov, "Kinetic-inductance-limited reset time of superconducting nanowire photon counters," *Appl. Phys. Lett.*, vol. 88, pp. 111116-1–111116-3, Mar. 2006.

[41] W. Słysz, M. Wegrzecki, J. Bar, P. Grabiec, M. Górska, V. Zwiller, C. Latta, P. Bohi, A. J. Pearlman, A. S. Cross, D. Pan, J. Kitaygorsky, I. Komissarov, A. Verevkin, I. Milostnaya, A. Korneev, O. Minayeva, G. Chulkova, K. Smirnov, B. Voronov, G. Gol'tsman, and R. Sobolewski, "Fibre-coupled single-photon detector based on NbN superconducting nanostructures for quantum communications," *Special Issue Single-Photon: Sources, Detectors, Appl., Meas. Methods, J. Mod. Opt.*, vol. 54, pp. 315–326, 2007.

[42] J. Kitaygorsky, I. Komissarov, A. Jukna, O. Minaeva, N. Kaurova, A. Korneev, B. Voronov, I. Milostnaya, G. Gol'tsman, and R. Sobolewski, "Dark counts in nanostructured NbN superconducting single-photon detectors and bridges," *IEEE Trans. Appl. Supercond.*, vol. 17, no. 2, pp. 275–278, 2007.

[43] A. Engel, A. D. Semenov, H.-W. Hübers, K. Il'in, and M. Siegel, "Fluctuation effects in superconducting nanostrips," *Physica C*, vol. 444, pp. 12–18, 2006.

[44] A. Semenov, A. Engel, K. Il'in, G. Gol'tsman, M. Siegel, and H.-W. Hübers, "Ultimate performance of a superconducting quantum detector," *Eur. Phys. J. AP*, vol. 21, pp. 171–178, 2003.

[45] H. Takesue, S. W. Nam, Q. Zhang, R. H. Hadfield, T. Honjo, K. Tamaki, and Y. Yamamoto, "Quantum key distribution over a 40-dB channel loss using superconducting single-photon detectors," *Nature Photonics*, vol. 21, pp. 343–348, 2007.

Elisabeth Reiger received the Graduate degree from the University of Regensburg, Regensburg, Germany, in 1999, and the Ph.D. degree from the University of Vienna, Vienna, Austria, in 2005, both in physics.

She was a Software Engineer in the automobile industry for one and a half years. She is currently a Postdoctoral Researcher at Delft University of Technology, Delft, The Netherlands, where she is engaged in the field of quantum optics. Her current research interests include superconducting single-photon detectors (SSPDs) that comprise fabrication, characterization, and investigation of new aspects of SSPDs.

Sander Dorenbos received the B.S. and M.S. degrees in 2006 and 2007, respectively, from Delft University of Technology, Delft, The Netherlands, where he is engaged in research on the fabrication and characterization of superconducting single-photon detectors.

Valery Zwiller received the Graduate degree from Strasbourg University, Strasbourg, France, in 1996, and the Ph.D. degree in single quantum dot optics from Lund University, Lund, Sweden, in 2001.

He was at Humboldt University, Berlin, and EPFL Lausanne and ETH Zurich, Switzerland. In 2005, he joined Delft University of Technology, Delft, The Netherlands, where he is currently an Assistant Professor. His current research interests include quantum optics and semiconductor nanostructures at the single photon level.

Alexander Korneev received the Graduate and Ph.D. degrees in radio-physics from the Moscow State Pedagogical University (MSPU), Moscow, Russia, in 2000 and 2006, respectively.

He is currently a Senior Scientist at the Radio-Physics Research and Educational Center, Department of Physics, MSPU. His research interests include studies of nonequilibrium processes in superconducting single-photon detectors.

Galina Chulkova received the M.S. degree in physics and the Ph.D. degree in solid-state physics from Moscow State Pedagogical University (MSPU), Moscow, Russia, in 1982 and 1997, respectively.

She is currently an Associate Professor in the Department of Physics, MSPU, where she is also a Senior Scientist at the Radio-Physics Research and Educational Center. She has been engaged in solid-state physics and electronics, electron–phonon interaction in disordered metals, films and 2-D heterostructures, and hot electron bolometers based on superconducting films. Her current research interests include the physics of superconducting nanostructures and superconducting single-photon detectors.

Irina Milostnaya received the M.S. degree in optical engineering from St. Petersburg State University of Information Technologies, Mechanics and Optics, St. Petersburg, Russia, in 1985, and the Ph.D. degree in radio-physics from Moscow State Pedagogical University (MSPU), Moscow, Russia in 1999.

She is currently an Associate Professor in the Department of Physics, MSPU, where she is also a Senior Scientist at the Radio-Physics Research and Educational Center. She has been engaged in studies on the influence of the laser radiation and current pulses on superconducting films, and nonequilibrium phenomena in superconductors. Her current research interests include the physics of superconducting nanostructures and superconducting single-photon detectors.

Olga Minaeva received the M.S. degree in physics in 2005 from Moscow State Pedagogical University (MSPU), Moscow, Russia, where she is currently working toward the Ph.D. degree in radio physics.

Her current research interests include the study of nonequilibrium phenomena in superconducting single-photon detectors. She is also engaged in the development and characterization of fast superconducting single-photon detectors.

Gregory Gol'tsman received the M.Sc. degree in physics, the Ph.D. degree in radio-physics, and the D.Sc degree in physics of semiconductors and Dielectrics from Moscow State Pegagogical University (MSPU), Moscow, Russia, in 1968, 1973, and 1985, respectively.

He is currently the Head of the Chair and the Head of the Radio-Physics Research and Educational Center at the Department of Physics, MSPU. He has been engaged in the field of solid-state physics and electronics, electron–phonon interaction and the hot-electron effect in metal and superconductors, kinetics of nonequilibrium superconductors, and physical mechanisms and transport in superconductors and superconducting devices, specifically, in hot electron bolometers, mixers, and detectors for submillimeter, far-infrared, and visible radiation.

Jennifer Kitaygorsky received the M.S. degree in 2005 from the Department of Electrical and Computer Engineering, University of Rochester, Rochester, NY, where she is currently working toward the Ph.D. degree.

Her current research interests include single-photon optical detectors, quantum cryptography, and dissipation in low-dimensional superconductors.

Dong Pan received the Double-Bachelor's degrees in law and physics from Nankai University, Tianjin, China, both in 1998, and the Double-Master's degrees in physics from the University of Rochester, Rochester, NY, from the Department of Physics in 2003, and in optics from the Institute of Optics in 2005, University of Rochester, where he is currently working toward the Ph.D. degree in physics at the Laboratory for Laser Energetics.

His current research interests include superconducting single-photon detectors, femtosecond lasers, pumped-entangled photon sources, and time-resolved photoresponse of nanostructured weak ferromagnet-superconductor bilayers.

Wojtek Słysz received the M.S. degree in electronic engineering from Warsaw University of Technology, in 1974, and the Ph.D. degree from the Institute of Electron Technology, Warsaw, Poland, in 2006.

He is currently with the Institute of Electron Technology. He has been engaged in activities on the semiconductor optical detectors and on other optoelectronic devices. His current research interests include quantum detectors, superconductor nanostructures, and related problems.

Arturas Jukna received the M.S. and Ph.D. degrees from Vilnius University, Vilnius, Lithuania, in 1985 and 1992, respectively, both in physics.

During 1996–1998, he was a Postdoctoral Fellow at the Royal Institute of Technology, Stockholm, Sweden. During 2002–2003, he was a Fulbright Scholar at the University of Rochester, Rochester NY. He is currently a Senior Research Associate at the Semiconductor Physics Institute and the Docent at the Vilnius Gediminas Technical University, Vilnius. His current research interests include ultrafast processes in photomaterials and optoelectronic devices, coherent motion of Abrikosov vortices in laser-written channels of high-critical-temperature (T_c) superconducting thin films, and control of ultra-wideband antenna radiation driven by the ultrafast photoresponse of the high-T_c superconducting thin films.

Roman Sobolewski received the Ph.D. and Sc.D. (Habilitation) degrees in physics from the Polish Academy of Sciences, Warsaw, Poland, in 1983 and 1992, respectively.

Between 1975 and 1990, he was with the Institute of Physics, Polish Academy of Sciences. In 1990, he joined the University of Rochester, Rochester, NY, where he is currently a Professor of electrical and computer engineering, physics, and materials science, as well as a Senior Scientist in the Laboratory for Laser Energetics, where he is the Head of the Ultrafast Quantum Phenomena Laboratory. His current research interests include the ultrafast and coherent phenomena in condensed matter, novel electronic, optoelectronic, and magnetic materials and devices, and quantum communications and computation. He is the author or coauthor of more than 300 peer-reviewed publications and has presented more than 100 invited talks, lectures, and colloquia worldwide. He is a Scientific Reviewer for several U.S. Government agencies and many professional journals.

Prof. Sobolewski he was the Organizer and a Co-Director of the NATO Advanced Research Workshop on Advanced Materials, Warsaw, Poland, in 2004. He obtained the State Professorship of the Republic of Poland in 2006. He is also a Consultant-Lecturer for the United Nations Industrial Development Organization.